

Correspondence: M. D. Ding (dmd@nju.edu.cn)

H α and hard X-ray observations of a two-ribbon flare associated with a filament eruption

M. D. Ding, Q. R. Chen, J. P. Li, and P. F. Chen

Department of Astronomy, Nanjing University, Nanjing 210093, China

ABSTRACT

We perform a multi-wavelength study of a two-ribbon flare on 2002 September 29 and its associated filament eruption, observed simultaneously in the H α line by a ground-based imaging spectrograph and in hard X-rays by RHESSI. The flare ribbons contain several H α bright kernels that show different evolutionary behaviors. In particular, we find two kernels that may be the footpoints of a loop. A single hard X-ray source appears to cover these two kernels and to move across the magnetic neutral line. We explain this as a result of the merging of two footpoint sources that show gradually asymmetric emission owing to an asymmetric magnetic topology of the newly reconnected loops. In one of the H α kernels, we detect a continuum enhancement at the visible wavelength. By checking its spatial and temporal relationship with the hard X-ray emission, we ascribe it as being caused by electron beam precipitation. In addition, we derive the line-of-sight velocity of the filament plasma based on the Doppler shift of the filament-caused absorption in the H α blue wing. The filament shows rapid acceleration during the impulsive phase. These observational features are in principal consistent with the general scenario of the canonical two-ribbon flare model.

Subject headings: line: profiles — Sun: filaments — Sun: flares — Sun: X-rays, gamma-rays

1. Introduction

Two-ribbon flares are usually accompanied by the eruption of filaments or coronal mass ejections (CMEs). A generally accepted model for two-ribbon flares predicts that prior to the flare, a filament (prominence) lies above magnetic arcades, which becomes unstable

owing to some processes such as a shear motion of magnetic arcades (Mikić & Linker 1994), a converging motion of them (Forbes & Priest 1995), or an emerging flux (e.g., Chen & Shibata 2000). The filament eruption leaves below a current sheet where magnetic reconnection occurs and energy is released to power a solar flare. Recently, the relationship between flares and filament eruptions (or CMEs) has become a hot topic (e.g., Zhang et al. 2001; Wang et al. 2003).

A two-ribbon flare comprises of a series of arcade loops whose footpoints form the two flare ribbons that are most often observed in $H\alpha$. It is known from observations with high spatial resolution that several flare kernels can appear in one ribbon, which correspond to different flaring loops whose energy processes (heating mechanisms) may be different (e.g., Kitahara & Kurokawa 1990). Asai et al. (2003) even identified small-scale conjugate footpoints in the two ribbons of a flare by searching for the most correlated $H\alpha$ light curves. Discrimination between different heating mechanisms (electron bombardment versus heat conduction) relies on several ways. First, as is well known, the hard X-ray emission provides a direct information on the site where high-energy electrons precipitate. Second, the emission features of the $H\alpha$ line can also be used as an indirect diagnostic tool for the heating mechanisms, based on the line shape and width (e.g., Canfield, Gunkler, & Ricchiazzi 1984; Canfield & Gayley 1987; Fang, Hénoux, & Gan 1993) and the comparison of $H\alpha$ and hard X-ray light curves (e.g., Wang et al. 2000; Trottet et al. 2000). In a few cases, heating at deeper layers can be achieved that produces an enhanced white-light emission. A probable cause is chromospheric heating by a strong electron beam followed by the backwarming effect (Liu, Ding & Fang 2001; Ding et al. 2003).

In this paper, we perform a multi-wavelength study of a two-ribbon flare on 2002 September 29, observed simultaneously by the Solar Tower Telescope of Nanjing University and the Reuven Ramaty High Energy Solar Spectroscopic Imager (RHESSI). The following topics are in particular addressed: (1) spatial and temporal variation of the $H\alpha$ and continuum emission; (2) dynamics of the filament eruption in association with the flare development; and (3) distribution of the hard X-ray source and its variation with time.

2. Observations

A two-ribbon flare (importance M2.6/2N), associated with a filament eruption, occurred at N12 E21 in NOAA Active Region 0134, on 2002 September 29. It started from 06:32 UT and peaked at 06:39 UT. We made spectral observations in $H\alpha$ and Ca II 8542 Å lines for this flare during the period of 06:35–06:49 UT, using the imaging spectrograph installed in the Solar Tower Telescope of Nanjing University (Huang et al. 1995; Ding et al. 1999).

Two-dimensional spectra for the whole flaring region were obtained by using a scanning technique. A frame of two-dimensional spectra contains a three-dimensional data array: 260 wavelength points around the line, 120 points along the slit with a pixel spacing $0''.85$, and 50 points along the scanning direction with a spacing $2''$. The spectral resolution is 0.05 and $0.118 \text{ \AA pixel}^{-1}$ for $H\alpha$ and $\text{Ca II } 8542 \text{ \AA}$ respectively. Therefore, we can detect the emission at the far wings of the lines ($\Delta\lambda = 6 \text{ \AA}$ for $H\alpha$ and 15 \AA for $\text{Ca II } 8542 \text{ \AA}$), which can be served as a proxy of the continuum window. We repeated in total 17 scans with a repetition time about 15 s in the impulsive phase. The last scan was done well after the flare when the continuum emission has dropped back to the quiescent value.

This flare was also observed by RHESSI, which provides the first high-resolution hard X-ray imaging spectroscopy (Lin et al. 2002). The hard X-ray data yield important information on high-energy electrons and the heating of the flare atmosphere. In addition, we use the data from the Michelson Doppler Imager (MDI) on board the *Solar and Heliospheric Observatory* (*SOHO*) to deduce the magnetic geometry related to this flare.

Reduction of the ground-based data includes a correction for the dark field and the flat field. $H\alpha$ images of the flaring region are reconstructed from the 2D spectral data. To compare images from different instruments, we align the $H\alpha$ image at the line wing with the MDI intensity image by tracing the sunspot features in the active region. The accuracy of image alignment is estimated to be $\sim 2''$. Other images can be overlapped similarly.

3. Results and Discussions

3.1. Evolution of the flare ribbons and the emission features

Figure 1 shows the $H\alpha$ monochromatic images (at the line center) of the 2002 September 29 flare at some selected times covering the impulsive phase. Overlapped is the magnetic neutral line from the MDI magnetogram observed at 06:24:01 UT, ~ 15 min prior to the flare maximum time. Therefore, when drawing the magnetic neutral line, we have applied a correction of 15 min solar rotation for consistency between the $H\alpha$ image and the magnetogram. It is seen that the curved magnetic neutral line divides the flare into three parts. The lower part below the neutral line is a small (fainter) ribbon. The upper part (above the neutral line) and the middle part (surrounded by the neutral line) look like to form a big (brighter) ribbon. However, they lie in areas of different magnetic polarities. In particular, we draw attention to two points across the neutral line, labeled as “A” and “B” in Fig. 1, and plot the time profiles of the $H\alpha$ emission in Fig. 2. Point “A” is the center of the kernel in the upper part of the flare and point “B” is the center of the kernel in the middle part

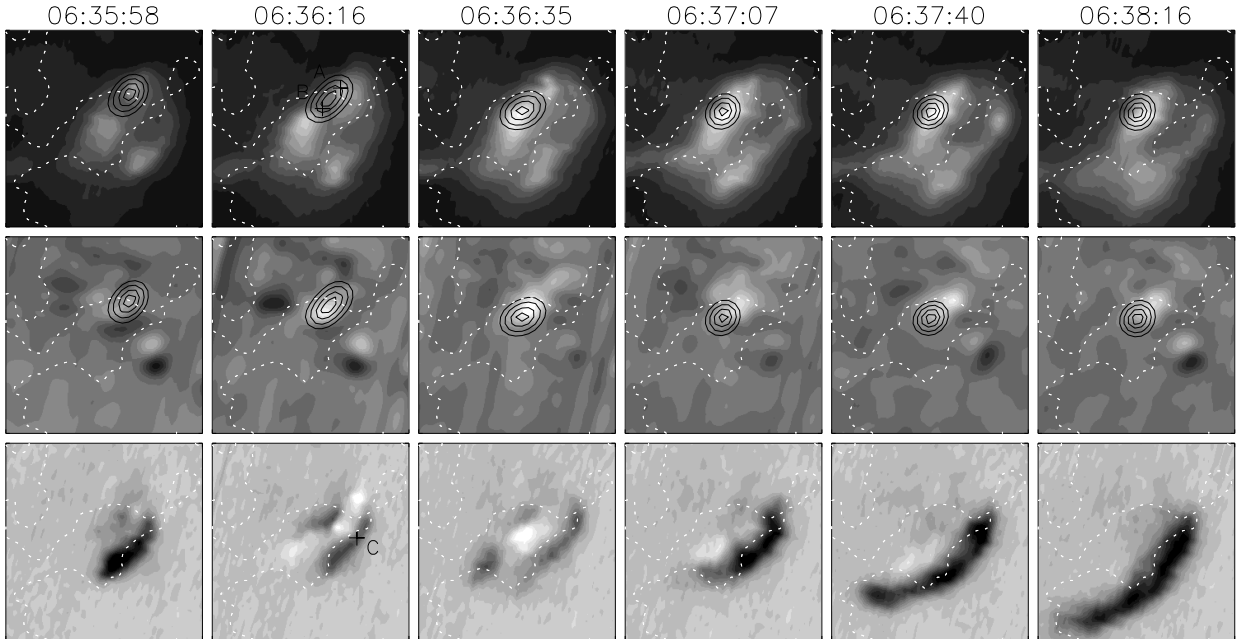


Fig. 1.— Images showing the evolution of the 2002 September 29 flare. *Top panel*: images at the $H\alpha$ line center; *middle panel*: images at $H\alpha + 6 \text{ \AA}$ as a proxy of the continuum emission; and *bottom panel*: difference of the $H\alpha - 4 \text{ \AA}$ and $H\alpha + 4 \text{ \AA}$ images showing the motion of the filament. The RHESSI hard X-ray contours (12–25 keV) are superimposed on the top and middle panels at each time. The magnetic neutral line, observed by *SOHO*/MDI, is also plotted as a white dotted line. “A”, “B”, and “C” are selected points that we refer to in Fig. 2. The field of view is $60'' \times 60''$. North is up, and east is to the left.

(also the brightest kernel in the flare). We find that point “A” is already relatively hot at the start of observations. It then cools down gradually with time. Point “B”, however, is relatively cool at first and is heated rapidly during the impulsive phase.

As mentioned above, a two-ribbon flare may consist of many small loops that flare up and evolve differently, and that produce light curves of different shapes. Generally speaking, the $H\alpha$ line emission originates from and reflects a heating status in the upper chromosphere, while the white-light continuum emission is from the lower chromosphere or photosphere. For the present event, we also search for the continuum emission near the $H\alpha$ line. We select a wavelength window at the far red wing (i.e., 6 \AA from the line center) to avoid a possible effect of the filament absorption, and then derive the relative enhancement of the intensity, defined as $R = (I_f - I_q)/I_q$, where I_f is the intensity during the flare and I_q is the quiescent value at the same point. The latter is taken as the intensity well after the flare (~ 10 min after the flare maximum). The same is done for the continuum near the $\text{Ca II } 8542 \text{ \AA}$ line,

but we use the wavelength window at 15 \AA from the line center. The time variations of the $\text{H}\alpha$ line center intensity and the continuum intensity for points “A” and “B” are plotted in Fig. 2, together with the RHESSI hard X-ray counts summed over detectors 1 through 9, excluding detectors 2 and 7.

We detect a fairly strong continuum enhancement ($R \approx 8 \%$) at point “B”. The continuum emission rises more rapidly than the line emission; it reaches a maximum that corresponds roughly to the peak of $\gtrsim 25 \text{ keV}$ hard X-ray emission, or a sub-peak of the hard X-ray emission at lower energies; then, it keeps above the quiescent value until the later phase of the flare. Note that we find a similar enhancement with a slightly less magnitude at the continuum near the $\text{Ca II } 8542 \text{ \AA}$ line. The visible continuum at point “A” seems also enhanced but much less significant than at point “B”. As will be discussed below, such a continuum emission may be related to electron beam precipitation.

We further study the origin of the hard X-ray emission by making a fit to the RHESSI hard X-ray spectra. Figure 3 plots the spatially integrated, background-subtracted photon spectrum for the time interval 06:36:00–06:37:00 UT, obtained using the RHESSI spectral executive software (Smith et al. 2002). We fit this spectrum by a bremsstrahlung spectrum that originates from both a thermal source and a thick-target source, as was done in Sui et al. (2002). The thick-target source yields a power-law fit. The results show that the non-thermal contribution to the hard X-ray emission dominates over the thermal source when $E \gtrsim 14 \text{ keV}$; the former becomes nearly one order of magnitude stronger than the latter at $E \sim 20 \text{ keV}$.

3.2. The filament eruption

The 2002 September 29 flare is closely associated with a filament eruption. In the observed $\text{H}\alpha$ and $\text{Ca II } 8542 \text{ \AA}$ spectra, the filament causes an absorption, or sometimes an emission, in the line blue wing. To view this feature clearly, we subtract the $\text{H}\alpha$ images at the red wing ($\Delta\lambda = 4 \text{ \AA}$) from that at the blue wing ($\Delta\lambda = -4 \text{ \AA}$) and plot these difference images in Fig. 1. The figure shows clearly the location and evolution of the filament (more accurately, the moving material in the filament). Seen from the MDI magnetogram overlapped on the image, the filament lies along the magnetic neutral line. With the flare development, the filament expands along its axis, in the southeastern direction. This phenomenon can be explained as a projection of the motion of the filament mass in the plane perpendicular to the line of sight. Since we cannot determine the velocity vector, we are unable to trace a specific mass element and study its dynamics. Therefore, we try to deduce the line-of-sight velocity for a fixed spatial point within the filament, based on the Doppler shift of the absorption

feature in the line wing. The time history of the line-of-sight velocity for a typical point in the midst of the filament, marked as “C” in Fig. 1, is shown in Fig. 2. The filament is shown to undergo a drastic acceleration during the impulsive phase; it reaches a maximum line-of-sight velocity of $\sim 210 \text{ km s}^{-1}$ at $\sim 06:37:40 \text{ UT}$, roughly in coincidence with the $\text{H}\alpha$ maximum at point B; after this, the filament is decelerated, while it continues to rise higher until the later phase of the flare.

The relationship between filament eruptions and flares has been extensively studied for decades (e.g., Rust 1976; Hanaoka et al. 1994; Wang et al. 2003). For a limb event, one can accurately determine the height of the erupting filament (prominence) and derive its propagation speed (e.g., Klein & Mouradian 2002). Since the event studied here is close to the disk center, it is hard to measure the height of the filament. The velocity derived from the Doppler shift of the absorption center reflects only a mean velocity averaged over the line of sight; it more probably corresponds to the velocity in the base part of the filament where the mass density is higher and most absorption is produced. However, the fact that the acceleration phase of the filament eruption corresponds to the flare impulsive phase provides a convincing confirmation of the result of Zhang et al. (2001).

We also notice from Fig. 1 (*the lower panels*) that the filament does not always appear in absorption (dark features); in stead, some parts may appear in emission (bright features) in the $\text{H}\alpha$ blue wing. This implies either an ejection of heated plasma (Batchelor & Hindsley 1991) or a heating of the filament material during its eruption. Note that such an emission feature appears especially in the impulsive phase.

3.3. The hard X-ray source and its motion

The spatial distribution and the temporal evolution of the hard X-ray emission provide clues to the acceleration of energetic electrons and to the heating of the flaring atmosphere. When a flare occurs, electrons are accelerated in the magnetic reconnection site and then precipitate downward along the magnetic field lines to both footpoints of the flaring loop, producing hard X-ray emission there. Therefore, in most cases, flares exhibit double hard X-ray sources (Sakao 1994), or multiple sources in the case of more than one flaring loops. However, in quite a few cases, only a single source is seen. This is either because the two footpoint sources are too close to be spatially resolved, or due to an asymmetric magnetic topology, in which the magnetic field in one loop leg is so converging that the magnetic mirroring effect inhibits most electrons from streaming downward.

The RHESSI data provide a good opportunity to study the above issue. To this end,

we construct the hard X-ray images at different times that are overlaid on the $H\alpha$ images in Fig. 1. In producing the hard X-ray images, we adopt the clean procedure, set the integration time to 12 s, and include detectors 3 through 8. We notice that a strong hard X-ray source appears, covering the bright points “A” and “B”, from the impulsive phase to the gradual phase. In the fainter ribbon, however, we only detect a rather weak source at the very beginning ($\sim 06:35$ – $06:36$ UT), prior to the $H\alpha$ observation time. This weak source is of a very short duration, located in the southeastern part of the fainter ribbon, which seems to have no relation to the strong source. Therefore, we think that the strong source itself contains two footpoint sources that are spatially mixed. A fact supporting this point is that the source straddles over the magnetic neutral line at earlier times (Fig. 1).

A further inspection of Fig. 1 reveals a motion of the hard X-ray source across the magnetic neutral line in the early phase. For a quantitative view, we plot in Fig. 4 the position of the centroid of the source at different energy bands for 5 successive time intervals of 12 s during $06:36$ – $06:37$ UT. Note that the centroid is defined as the intensity-weighted center of the hard X-ray source with $\geq 50\%$ peak intensity. Since the shape of the hard X-ray source is nearly round, the centroid is roughly the place of peak intensity. The source motion is seen to depend on the energy of the emission. The source at a higher energy band moves later, but across a longer distance, than that at a lower energy band. Note that such a difference can be explained by the different proportions of thermal and non-thermal sources at different energy bands. As revealed in Fig. 3, the hard X-ray emission at 3–12 keV is mainly thermal, while that at 25–50 keV is nearly nonthermal; at 12–25 keV, the thermal and nonthermal contributions are comparable. (In fact, we have also tried to construct the hard X-ray image at the 50–100 keV range; however, the centroid of the source cannot be reliably determined since the count rates are not large enough.) To trace the fastest source motion, we shorten the time interval (also the integration time) to as small as 2 s; at the 25–50 keV band, the biggest motion during this small interval is $\gtrsim 2''$, which means a source motion speed as large as $\gtrsim 1''$ per second. We also find that at first, the sources at different energy bands are more spatially separated than later; they converge to nearly the same place and become relatively stable after their motions stop (at $\sim 06:37$ UT).

Sakao et al. (2000) have studied in detail the motion of hard X-ray (double) sources in flares observed by *Yohkoh*. They found that in most cases, the double sources move antiparallely. Krucker, Hurford, & Lin (2003) also found a hard X-ray source motion roughly parallel to the magnetic neutral line with a velocity of up to ~ 100 km s $^{-1}$. Masuda, Kosugi, & Hudson (2001) found both kinds of hard X-ray source motions, parallel and vertical to the magnetic neutral line, for an X-class flare. In our case, the source motion does show both the parallel and vertical components. Note that at the 25–50 keV energy band, the motion is nearly perpendicular to the magnetic neutral line during the period of fast motion. Since

this source is probably a merging of two footpoint sources, we propose two causes for such a motion: an asymmetric hard X-ray emission, that is, the footpoint source at the southern side of the neutral line gradually dominates over that at the northern side, and/or a ribbon separation from the neutral line (e.g., Qiu et al. 2002). We think that the first effect is more important during the short period of fast motion. That is to say, there is a mechanism that suddenly switches off (or greatly reduces) the emission from the northern side but enhances the emission from the southern side. We further postulate that the magnetic topology of the newly reconnected loops becomes very asymmetric so that the magnetic mirroring effect results in such an asymmetric hard X-ray emission.

To confirm the above point, we compute the magnetic topology of the active region from the MDI magnetogram using a potential field extrapolation developed by Sakurai (1982). In Fig. 5, we schematically plot the magnetic field lines projected on the MDI magnetogram. For clarity, only the field lines in the flaring region are given. The connectivity of the magnetic field indicates that there are magnetic loops that straddle over the upper part of the magnetic neutral line. These loops are responsible for the production of the main hard X-ray source and the continuum emission, as discussed above. In addition, there appear other loops that connect the $H\alpha$ brighter ribbon and the fainter ribbon (across the lower part of the magnetic neutral line). The overall picture of this flare is a sequence of sheared magnetic arcade loops and a filament lying above them. Unfortunately, the cadence of MDI magnetograms is only 96 min; therefore, we are unable to learn the magnetic field change during the flare.

Note that we do not find a corresponding motion of the continuum emission source. This is not surprising if we interpret the continuum emission as due to the backwarming effect (Ding et al. 2003). The lower atmosphere requires tens of seconds to get fully heated, so that the continuum emission cannot follow closely in space the fast motion of the hard X-ray emission. Of course, it may also be due to the relatively low spatial resolution of the 2D spectral observations.

4. Conclusions

We have studied the $H\alpha$ emission and the RHESSI hard X-ray emission of the 2002 September 29 flare. The main results are as follows.

(1) The flare is associated with a filament eruption. A rapid acceleration of the filament occurs in the flare impulsive phase. The line-of-sight velocity deduced at a fixed spatial point within the filament is seen to reach a maximum at nearly the same time of $H\alpha$ maximum

in the brightest kernel. In the impulsive phase, some parts of the filament may produce an emission in the $H\alpha$ blue wing. This implies either a heating of the filament mass or an ejection of heated plasma.

(2) The flare ribbons comprise of several $H\alpha$ kernels that evolve differently. Judging from the magnetic topology and the emission features in both $H\alpha$ and hard X-rays, we have identified two bright points, which lie at both sides of the magnetic neutral line and are probably the footpoints of a flaring loop.

(3) We detect a motion of the hard X-ray source across the magnetic neutral line. Since this source is probably a merging of two footpoint sources, its motion is ascribed to a rapid change of their relative weights owing to a change of the magnetic topology of the newly reconnected loops. However, it is still unclear what is the mechanism that produces such a change in a very short time (~ 2 s).

(4) We also detect an enhanced emission at the visible continuum (near $H\alpha$) and the infrared continuum (near $\text{Ca II } 8542 \text{ \AA}$), at a place near the center of the hard X-ray source. Liu et al. (2001) have reported a similar continuum emission in a flare of 2001 March 10. Ding et al. (2003) proposed a model for the continuum emission as a result of electron beam heating followed by radiative backwarming. The results here favor such an interpretation.

In principal, the observed features of this flare can still be interpreted by the canonical model of two-ribbon flares (Kopp & Pneuman 1976).

We would like to thank the referee for his/her valuable comments on the paper. We are grateful to the RHESSI team and the *SOHO*/MDI team for providing the observational data, and to T. Sakurai for providing the computer code for magnetic field extrapolation. This work was supported by NKBRSF under grant G20000784, by NSFC under grants 10025315 and 10221001, and by a grant from TRAPOYT.

REFERENCES

- Asai, A., Ishii, T. T., Kurokawa, H., Yokoyama, T., & Shimojo, M. 2003, *ApJ*, 586, 624
- Batchelor, D. A., & Hindsley, K. P. 1991, *Sol. Phys.*, 135, 99
- Canfield, R. C., & Gayley, K. G. 1987, *ApJ*, 322, 999
- Canfield, R. C., Gunkler, T. A., & Ricchiazzi, P. J. 1984, *ApJ*, 282, 296
- Chen, P. F., & Shibata, K. 2000, *ApJ*, 545, 524

- Ding, M. D., Fang, C., Yin, S. Y., & Chen, P. F. 1999, *A&A*, 348, L29
- Ding, M. D., Liu, Y., Yeh, C.-T., & Li, J. P. 2003, *A&A*, 403, 1151
- Fang, C., Hénoux, J.-C., & Gan, W. Q. 1993, *A&A*, 274, 917
- Forbes, T. G., & Priest, E. R. 1995, *ApJ*, 446, 377
- Hanaoka, Y., et al. 1994, *PASJ*, 46, 205
- Huang, Y. R., Fang, C., Ding, M. D., Gao, X. F., Zhu, Z. G., Ying, S. Y., Hu, J., & Xue, Y. Z. 1995, *Sol. Phys.*, 159, 127
- Kitahara, T., & Kurokawa, H. 1990, *Sol. Phys.*, 125, 321
- Klein, K.-L., & Mouradian, Z. 2002, *A&A*, 381, 683
- Kopp, R. A., & Pneuman, G. W. 1976, *Sol. Phys.*, 50, 85
- Krucker, S., Hurford, G. J., & Lin, R. P. 2003, *ApJ*, in press
- Lin, R. P., et al. 2002, *Sol. Phys.*, 210, 3
- Liu, Y., Ding, M. D., & Fang, C. 2001, *ApJ*, 563, L169
- Masuda, S., Kosugi, T., & Hudson, H. S. 2001, *Sol. Phys.*, 204, 55
- Mikić, Z., & Linker, J. A. 1994, *ApJ*, 430, 898
- Qiu, J., Lee, J., Gary, D. E., & Wang, H. 2002, *ApJ*, 565, 1335
- Rust, D. M. 1976, *Sol. Phys.*, 47, 21
- Sakao, T. 1994, Ph.D. thesis, Univ. Tokyo
- Sakao, T., Kosugi, T., Masuda, S., & Sato, J. 2000, *Adv. Space Res.*, 26, 497
- Sakurai, T. 1982, *Sol. Phys.*, 76, 301
- Smith, D. M., et al. 2002, *Sol. Phys.*, 210, 33
- Sui, L., Holman, G. D., Dennis, B. R., Krucker, S., Schwartz, R. A., & Tolbert, K. 2002, *Sol. Phys.*, 210, 245
- Trottet, G., Rolli, E., Magun, A., Barat, C., Kuznetsov, A., Sunyaev, R., & Terekhov, O. 2000, *A&A*, 356, 1067

Wang, H., Qiu, J., Denker, C., Spirock, T., Chen, H., & Goode, P. R. 2000, *ApJ*, 542, 1080

Wang, H., Qiu, J., Jing, J., & Zhang, H. 2003, *ApJ*, in press

Zhang, J., Dere, K. P., Howard, R. A., Kundu, M. R., & White, S. M. 2001, *ApJ*, 559, 452

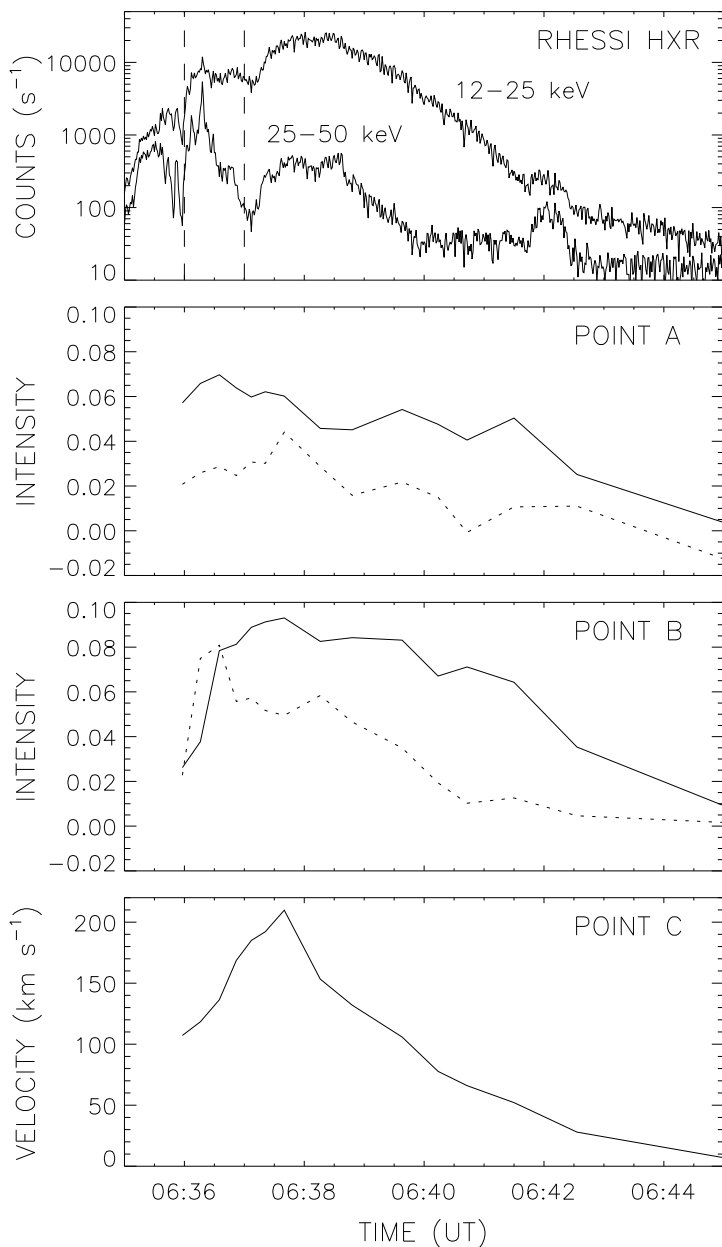


Fig. 2.— Time profiles of the RHESSI hard X-ray emission at 12–25 and 25–50 keV energy bands (*top panel*), the net increase of the emission at $H\alpha$ line center (*solid line*) and at $H\alpha + 6 \text{ \AA}$ (*dotted line*), normalized to the quiescent intensity at $H\alpha + 6 \text{ \AA}$, at points “A” and “B” (*middle panels*), and the line-of-sight velocity at point “C” in the filament (*bottom panel*). The two vertical bars in the top panel refer to the integration time interval for which the photon spectrum is generated (Fig. 3).

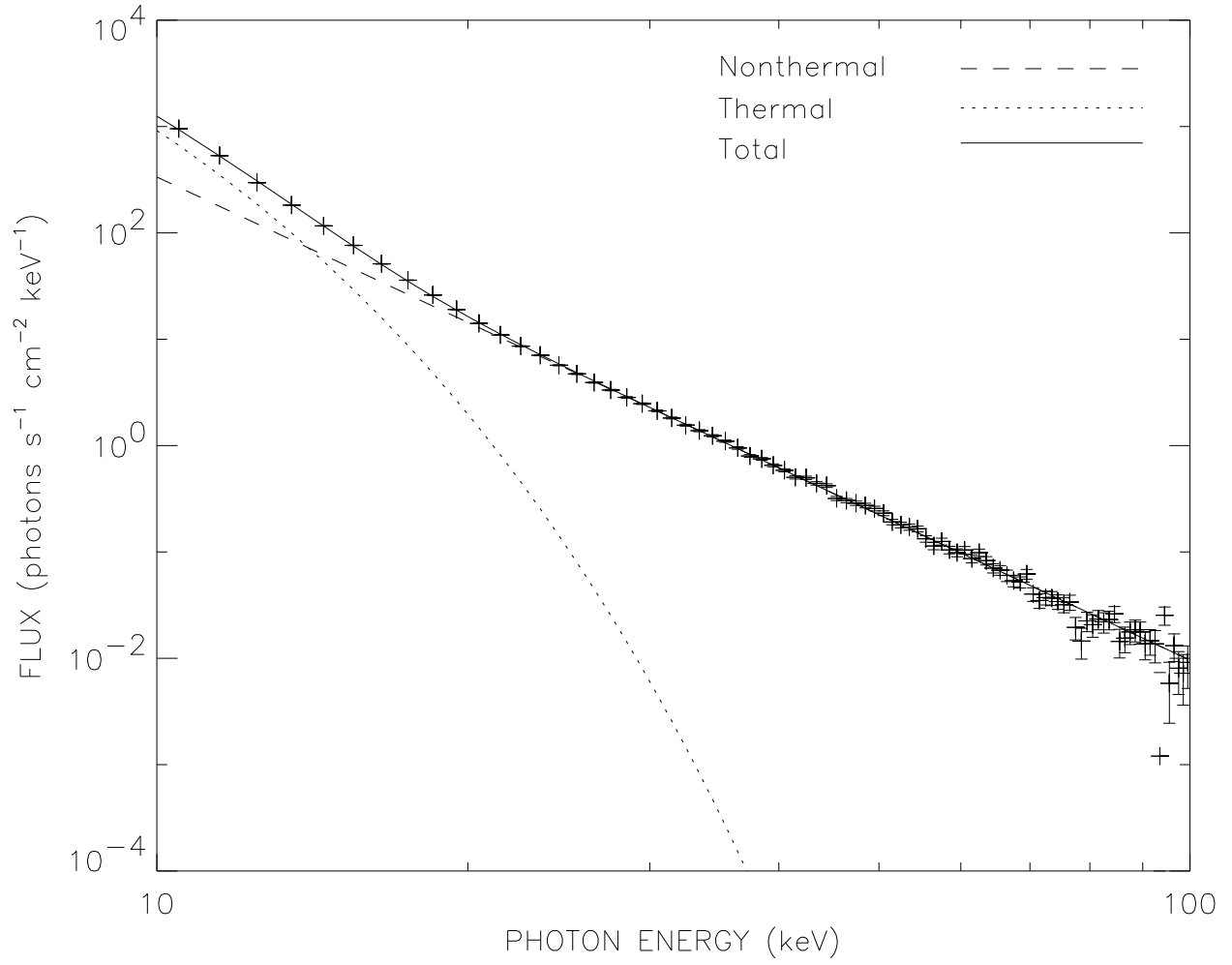


Fig. 3.— RHESSI photon spectrum for the time interval 06:36:00–06:37:00 UT, fitted by the spectrum from a thermal source plus a thick-target source.

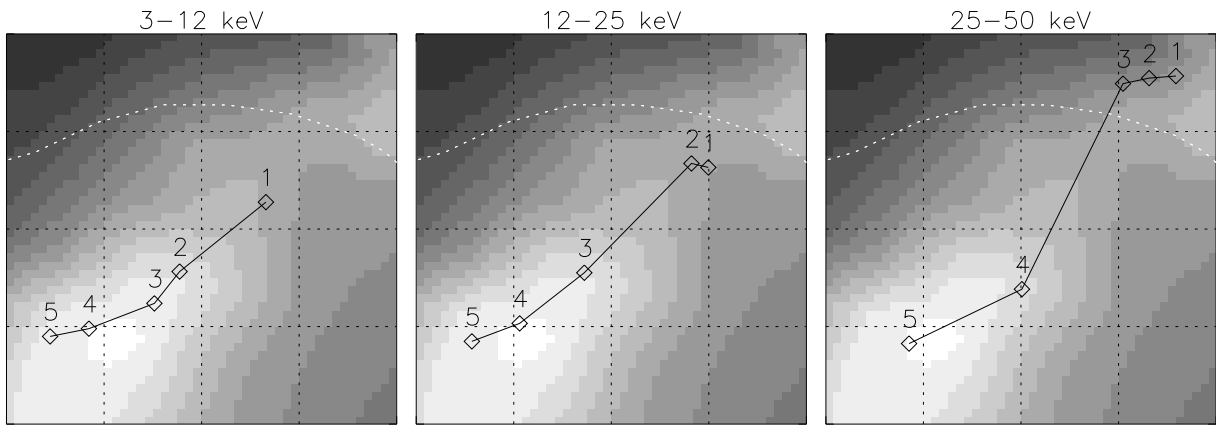


Fig. 4.— Position of the centroid of the main hard X-ray source at 5 consecutive time intervals of 12 s between 06:36:00 and 06:37:00 UT (*diamonds*), and the magnetic neutral line (*white dotted line*) overlaid on the flare image at 06:36:35 UT. The field of view is $12'' \times 12''$.

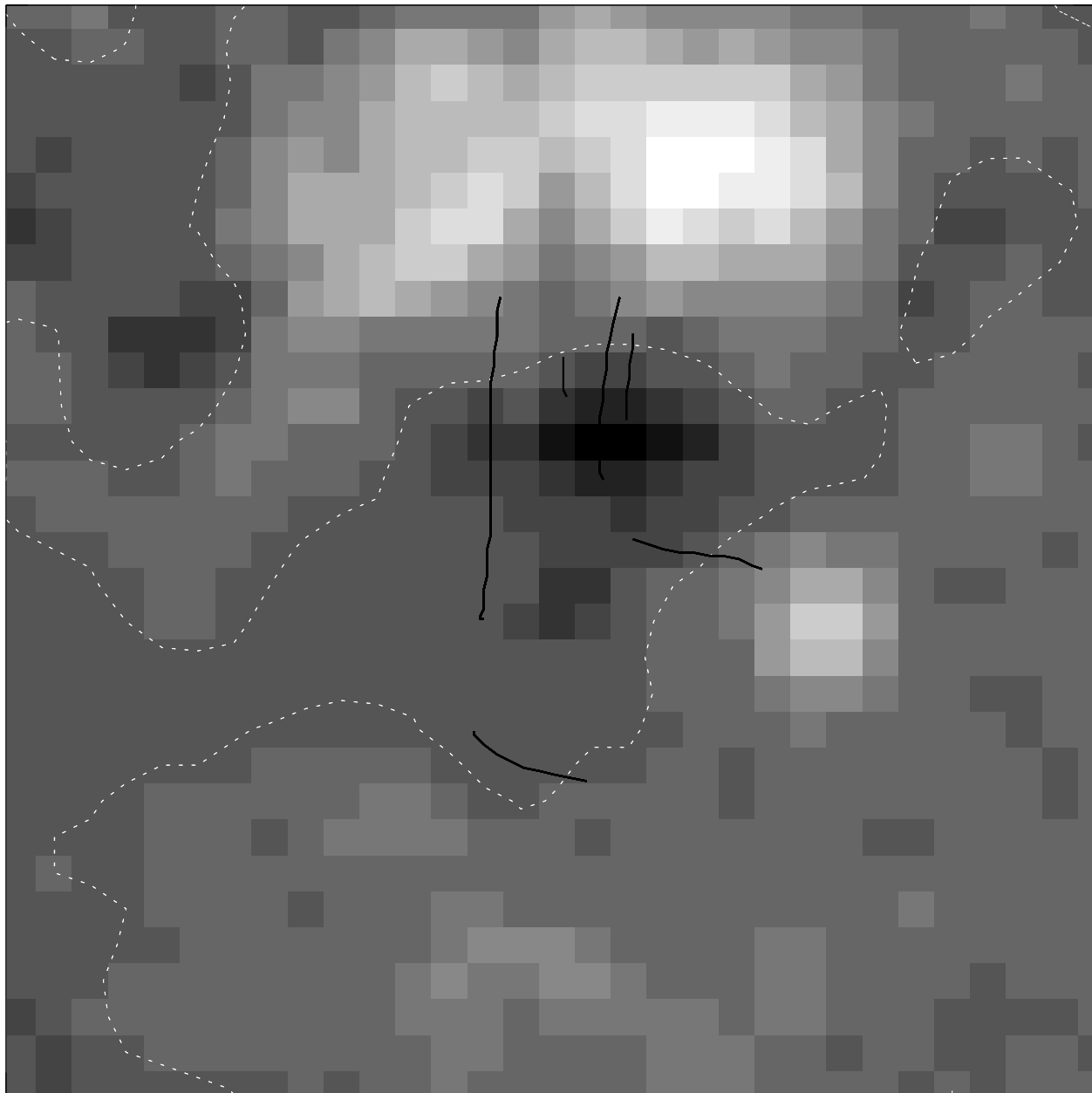


Fig. 5.— Magnetic field lines computed using a potential field extrapolation from the MDI data (*solid line*). Also plotted are the MDI magnetogram (*gray scale*) and the magnetic neutral line (*white dotted line*). The field of view is $60'' \times 60''$.